Electrochimica Acta 231 (2017) 529–538

Contents lists available at ScienceDirect

Electrochimica Acta

journal homepage: www.elsevier.com/locate/electacta

Effect of the solvent in the catalyst ink preparation on the properties and performance of unsupported PtRu catalyst layers in direct methanol fuel cells

Francisco Alcaide[a,*,1], Garbiñe Álvarez[a], Pere L. Cabot[b,1], Radostina Genova-Koleva[b], Hans-Jürgen Grande[a,1], Oscar Miguel[a]

[a] Energy Division, IK4-CIDETEC, P° Miramón, 196, 20009 San Sebastián, Spain
[b] Laboratory of Materials and Environmental Electrochemistry, Department of Materials Science and Physical Chemistry, Section of Physical Chemistry, Faculty of Chemistry, Universitat de Barcelona, Martí i Franquès, 1-11, 08028 Barcelona, Spain

ARTICLE INFO

Article history:
Received 27 July 2016
Received in revised form 21 February 2017
Accepted 21 February 2017
Available online 24 February 2017

Keywords:
direct methanol fuel cell
catalyst ink
PtRu black
catalyst layer
Nafion® ionomer

ABSTRACT

The effect of the organic solvent polarity on the properties of unsupported PtRu catalyst inks and on the performance of the catalyst layers prepared with them for the methanol electrooxidation, has been studied. The light scattering results indicate that the PtRu-Nafion® aggregates in the inks prepared with n-butyl acetate (NBA) are larger than those prepared with 2-propanol (IPA). The lower polarity of the former favours the aggregation of Nafion® and nanoparticles. The electron microscopy images and porosimetry measurements of the catalyst layers show that the secondary pore volume between the agglomerates is larger for NBA. The linear sweep voltammetry and *eis* results for the methanol electrooxidation in the three-electrode cell denote the higher active surface area for NBA and comparable specific oxidation rates of the intermediates in both catalysts layers. The current densities for PtRu anode catalyst layers in single DMFC are higher when the solvent is NBA, the mass transport limitations being much more apparent with IPA. The adapted transmission line equivalent circuit to interpret the impedance results in single DMFC indicates that the proton resistance for NBA is significantly lower than for IPA, thus suggesting that the greater number of accessible active sites for methanol oxidation in the former are well connected to the Nafion® ionomers and easier transported to the membrane.

1. Introduction

Polymer electrolyte membrane fuel cells (PEMFCs) are nowadays receiving much attention due to their attractive properties as a power source for both, stationary and mobile applications. Some of their main advantages are the absence of electrolyte leakage, low corrosion and simple stack design [1]. Liquid-feed direct methanol fuel cells (DMFCs) based on a Nafion® proton exchange membrane (PEM) appear to be the most promising for portable and low-power applications, because of their simple and compact design, lightweight, no need for hydrogen storage or a fuel reformer, no need of the hydrogen and air humidification, easy recharging and easy storage, distribution and management of the liquid alcohol [2].

It is known that the power output of a PEMFC is related to the electrode catalyst layers. In fact, one of the main challenges in this research field is the optimization of the electrode composition and morphology in order to improve the fuel cell performance and durability. Many attempts to improve the electrode manufacturing of H_2-fueled PEMFCs have been made [1,3–12], whereas those performed on DMFCs are comparatively smaller [2,13–18]. Thus, in H_2-fueled PEMFCs more attention has been paid in the literature to supported catalysts for increasing the active surface area and to obtain better cell performance [1,3–12,18,19]. In contrast, the use of unsupported catalysts is more extended in DMFCs. Unsupported catalysts or metal blacks are mainly utilized in systems operating in passive mode, that is, without any air blowers or fuel circulating pumps, such as in portable electronic applications [20–24] and related miniaturized systems [25–27]. In this sense, it has been reported that the best compromise between power density (21 mW cm^{-2}) and fuel efficiency (63%) for a passive single DMFC containing PtRu and Pt blacks is achieved with a methanol feed concentration of 2 mol dm^{-3} operating at room temperature [28].

* Corresponding author.
E-mail address: falcaide@cidetec.es (F. Alcaide).
[1] ISE members.

http://dx.doi.org/10.1016/j.electacta.2017.02.127
0013-4686/

With regard to DMFC systems operating in active mode, the performance depends largely on the experimental operating conditions. For an active DMFC 30-cell stack containing PtRu and Pt blacks fed with 0.48 mol dm^{-3} methanol solution and dry air at 7.35 slpm (standard litre per minute) and 0.76 atm, a power density of 63 mW cm^{-2} (0.467 V/cell) and fuel efficiency of 89% was reported operating at 60 °C [29]. More recently, for single DMFC with PtRu and Pt blacks, after discharging the cell at constant current density of 0.200 A cm^{-2} for 1450 h, a maximum power density of 37 mW cm^{-2} (0.306 V) was reported at 70 °C, decreasing from an initial value of 100 mW cm^{-2} (0.346 V), feeding the anode and cathode with 1 mol dm^{-3} methanol and air, respectively (both at stoichiometry λ = 6) [30]. Furthermore, an active single DMFC using supported catalysts was described showing a maximum power density of 180 mW cm^{-2} (0.300 V), at 80 °C and optimum operating conditions [31].

The technical interest in unsupported PtRu alloy catalysts is based on the fact that, in practical applications, it is expected that catalyst layers with reduced thickness show better performance, due to the improved mass transport and the decrease of the inner electrical resistance [32]. In these catalysts, Ru forms oxygenated species at lower potentials than platinum and promotes the oxidation of adsorbed CO molecules on platinum to CO_2, thus increasing the CO tolerance of the catalyst. At high concentrations, CO_2 can remain trapped inside the catalyst layer and therefore, mass transport limitations can appear. The use of unsupported catalysts facilitates the CO_2 transport because thinner active layers can be obtained in comparison to supported catalysts with similar catalysts loadings [33,34]. Furthermore, regarding durability issues, the use of unsupported catalysts avoids the problem of carbon corrosion [30,35].

As previously mentioned, the morphology and composition of the electrode plays an important role in the fuel cell performance. This issue is closely related to the dispersion techniques [3] and solvents [1,5,8–10,14] used in the catalyst inks for preparation of the electrode active layers in the MEAs (membrane electrode assemblies). It is known that the performance of a catalyst layer depends on the catalyst ink composition, the ink preparation procedure, and the application method onto a substrate to fabricate the MEA. Uchida and col. [5] reported the changes of the Nafion® layout in various kinds of organic media, depending on their dielectric constant. Thus, in organic solvents with $\varepsilon > 10$, a solution is formed; when $3 < \varepsilon < 10$, a colloidal solution results; and with $\varepsilon < 3$, precipitation occurs [1,5,14]. In the first case, it is considered that the ionomer can cover the surface of the carbon and, as the ionomer is an electron insulator, the Pt utilization decreases and the conduction of electrons is blocked. This possibility leads to low fuel cell performance. In the second case, the ionomer colloids adsorb the catalyst powder and the size of the agglomerates of catalyst powder increases. Then, the electrode porosity increases, and the mass transfer is facilitated. A continuous network of ionomer throughout the catalytic layer can be built up, thus improving the proton conduction from the electrode to the membrane and resulting in a better fuel cell performance [1,14]. It has been reported that the electrode prepared by colloid formation shows an increase of about 30% in the electrochemical reaction area and therefore, the cell performance is significantly improved when compared to the cell using electrodes prepared by the solution method. Another point is that when the colloid is formed, the ionomers can easily penetrate into the large pores and the small pores below 0.07 μm are not blocked. Conversely, all pores below 0.07 μm are blocked by ionomers in the case of the solution method [1].

An additional condition for producing a stable cast ionomer is related to the higher boiling point of the solvent with respect to water [14]. Even if ε of an organic solvent is larger than 10 and the perfluorosulfonated ionomer dissolves into the catalyst ink solution, a different type of organic solvent could form a different catalyst layer structure. This is because the pores in the catalyst layer are formed during the evaporation process of the catalyst ink, and the process depends on the physical and thermodynamic properties of the organic solvent [8]. Thus, it has been shown that the porosity of the catalyst layer can be tuned even when using solvents with $\varepsilon > 10$, although the difference in their viscosity and boiling points are essential in this case [8–10]. It is worth mentioning that, in the best of the authors' knowledge, the influence of the ink composition on the catalytic layer properties for PEMFCs has only been studied when using carbon supported catalysts. The study of the effect of the catalyst ink composition for unsupported catalysts would be also of interest since they are frequently used in DMFCs.

This work deals with the study of the solvent influence on the catalyst inks for active layer manufacturing in DMFC applications, to show whether the aforementioned considerations also apply for the unsupported catalysts. Two types of solvents, leading to the solution and to the colloidal methods discussed above, 2-propanol (IPA) and n-butyl acetate (NBA), respectively, have been used. The corresponding catalysts, characterized using physical methods, have been applied to single electrodes to study the methanol oxidation reaction using electrochemical techniques in a three-electrode configuration cell. In addition, MEAs have also been manufactured using the prepared catalysts layers to test their performance in single liquid-feed DMFCs.

2. Experimental

2.1. Porous diffusion electrodes

Porous diffusion anodes consist of a gas diffusion layer (GDL) and a catalyst layer (CL). The GDL was a thin layer made of Vulcan XC-72 (Cabot Corp.) carbon black and polytetrafluoroethylene deposited on the top of hydrofobized Toray carbon paper (TGPH-090, 20% wet proofing, E-TEK Inc.) [36]. A catalyst ink was prepared using the following procedure based on the "dropping process" reported by Uchida et al. for PEMFC electrodes [3]. First, the PtRu black catalyst (Pt:Ru; 50:50 at. %, HISPEC™ 6000, Alfa Aesar®) was wetted with ultrapure water ($\kappa \leq 0.054$ μS cm^{-1}, obtained from a Millipore System), and mixed with an organic solvent (see Table 1 for more details) under ultrasonic stirring for 30 min. Next, an appropriate amount of Nafion® dispersion (5% wt., Aldrich) was dropped into the catalyst solution while stirring to achieve a dry ionomer composition of 15 wt. % in the CL [37–40]. Ultrasonic stirring was applied for another 2 h at room temperature to obtain a uniform dispersion. Afterwards, the catalyst ink was sprayed onto the GDL by an air-gun feed with pure nitrogen (99.999%, Praxair) and dried at 60 °C in an oven. The PtRu black loading was adjusted to 4.0 mg cm^{-2}.

The gas diffusion cathode consists of an ELAT® V2.1 (E-TEK, Inc.) gas diffusion layer and a catalyst layer made of Pt black (HSA, Premetek Co.) at a loading of 4.0 mg cm^{-2} and Nafion® ionomer with a 10 wt. % by dry weight content. The CL was prepared

Table 1
Selected physical properties of the organic solvents used to prepare the catalyst inks.

Solvent	ε[a]	P_v[b]/hPa	T_b[c]/°C
n-butyl acetate (NBA)	5.01	13.0	126.5
2-propanol (IPA)	18.0	43.0	82.4

[a] Dielectric constant at 25 °C.
[b] Vapour pressure at 20 °C.
[c] Boiling temperature.

following the same method as for the anode, but the catalyst ink contained n-butyl acetate as organic solvent.

2.2. Membrane electrode assembly

MEAs of 5 cm^2 in active area section were prepared using the hot press method [41]. Nafion® 115 membranes (DuPont) were cleaned and converted into the acid form by boiling in 3% H_2O_2 for 1 h, followed by boiling in 0.5 mol dm^{-3} H_2SO_4 for 2 h, and finally boiling in ultrapure water for 2 h with the water being changed after every 30 min. The cleaned membrane was stored in ultrapure water and dried before use. Each MEA was assembled by hot-pressing the anode and cathode on either side of the pretreated membrane at 50 bar and 130 °C for 3 min. Previously, additional ionomer solution was sprayed onto the catalyst layer of each electrode at a loading of 0.80 mg cm^{-2} (dry basis).

2.3. Physical characterization

The X-ray diffraction technique (XRD) was used to characterize commercial PtRu and Pt black catalysts. The XRD diffractograms for bulk materials and electrodes [2] were obtained by a Bruker D8 Advance diffractometer operating with Cu Kα radiation (λ = 1.5406 Å) and a 2θ scan from 30 to 100° (at 0.02° min^{-1}). Diffraction peaks were assigned according to the International Centre for Diffraction Data (ICDD) cards in PDF-2 database. The XRD data were used to determine the lattice parameter (from the interplanar distances) and the average crystallite size (by using Scherrer equation) [42]. The mass ratio of Pt to Ru was analysed by the energy dispersive X-ray (EDX) technique. The EDX measurements were performed with an INCA-300 energy analyser coupled to a scanning electron JSM5910-LV JEOL microscope. The PtRu bulk composition was determined from the average of five different measurements on the same sample with relative errors less than 1%. The particle size distribution in the catalyst inks was measured by laser diffraction using a LS 13 320 (Beckman Coulter) particle size analyser. Scanning electron microscopy (SEM) images of the anode catalyst layers were taken using a JSM5910-LV JEOL microscope, and their pore size distributions were determined by a mercury porosimeter (Quantachrome Pore Master).

2.4. Electrochemical characterization and fuel cell testing

Methanol electrooxidation measurements were carried out in a thermostated two-compartment electrochemical glass cell. A N_2-purged solution of 2.0 mol dm^{-3} CH_3OH + 0.5 mol dm^{-3} H_2SO_4 was used as electrolyte. The working electrode, prepared according to subsection 2.1, was placed inside a holder, being 0.79 cm^2 the geometric area exposed to the solution. A gold mesh was used as the current collector. The reference electrode was $Hg|Hg_2SO_4$, K_2SO_{4sat} (0.700 ± 0.003 V vs. RHE in 0.5 mol dm^{-3} H_2SO_4), separated from the main solution compartment by a tube ended in a Luggin-Haber capillary. However, all the potentials in this work are quoted against the reversible hydrogen electrode (RHE). The counter electrode consisted of a Pt wire separated from the main solution by a fritted glass.

The electrochemical measurements were performed by means of a potentiostat PGSTAT 30 (Eco Chemie) driven by the GPES software. Before these measurements, the surface of the PtRu catalysed electrodes was cleaned by cyclic voltammetry (*cv*) between 0.075 and 0.750 V at 0.100 V s^{-1} in N_2-purged 0.5 mol dm^{-3} H_2SO_4 (Merck Suprapure) solution until observing a steady voltammogram (usually 25 cycles). Linear sweep voltammetry was performed between 0.075 and 0.750 V to avoid Ru dissolution. Electrochemical impedance spectroscopy (*eis*) measurements were carried out in the potentiostatic mode using a 1255 FRA combined with a 1287A potentiostat (both Solartron Analytical, Inc.), commanded by the CorrWare Electrochemical/Corrosion and Z-Plot impedance software. Impedance spectra were collected applying a potential of 0.400 V. The *ac* amplitude was 5 mV and the frequency ranged between 10 kHz and 0.010 Hz, with 10 steps dec^{-1}. The integration time was set at 10 s. The electrochemical active surface areas (ECSAs) were estimated from CO stripping voltammetry [43]. Before stripping, CO was first adsorbed onto the electrode surface at 0.100 V for 30 min and subsequently the electrolyte was purged by N_2 bubbling for 20 min.

On the other hand, each type of MEA was manufactured and tested by triplicate. Testing in single DMFC was performed using MEAs of 5 cm^2 in active area section, coupled to commercial fuel cell hardware (Fuel Cell Technologies, Inc.). The MEA, flanked by the two graphite current collectors with serpentine flow fields, was held between two gold-plated stainless-steel contact plates using a set of retaining bolts positioned around the periphery of the cell. A uniform clamping torque of 5 N m was applied. The anodic compartment of the cell was fed with 2.0 mol dm^{-3} aqueous methanol solution preheated at 60 °C, keeping the flow rate at 2.0 mL min^{-1}. Dry high purity synthetic air (Praxair, 99.999%) at fixed flow rate of 100 mL min^{-1} and atmospheric pressure, was fed through the cathodic compartment. The cell temperature was set at 60.0 °C. Steady-state *V-j* polarization curves were recorded from the open circuit voltage down to 0.1 V at scan rate of 1 mV s^{-1} by a 1287A potentiostat (Solartron Analytical, Inc.). Polarization curves with an error less than 5% in the overall current density range were obtained. To carry out in situ *eis* measurements and CO stripping, the MEA was operated in driven cell mode, *i.e.* the anode was the working electrode and the cathode was feed with hydrogen, acting as a counter and reference electrode (dynamic reference electrode, DHE). CO voltammetry stripping experiments were carried out at T_{cell} = 25 °C, feeding the anode with a mixture of 0.1% CO in N_2 and 250 cm^3 min^{-1} at atmospheric pressure for 50 min, while holding the electrode potential at 0.100 V vs. DHE. After adsorption, the gas was switched to N_2 for 20 min. at 250 cm^3 min^{-1} and the admission potential, to remove any CO from the single cell. The cathode was fed with humidified hydrogen at 200 cm^3 min^{-1}. All gases were humidified at T_{cell}. Two CO stripping voltammograms were then recorded in the positive direction at 20 mV s^{-1} [44].

3. Results and discussion

3.1. Physical characterization of the catalysts

XRD patterns of PtRu and Pt black commercial catalysts are shown in Fig. 1. This figure clearly shows the crystalline structure of the PtRu and the Pt catalysts nanoparticles. Both XRD spectra display the (111), (200), (220), (311), and (222) diffraction peaks

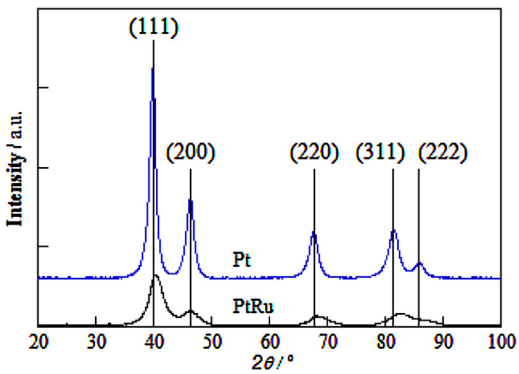

Fig. 1. X-ray diffraction patterns of PtRu and Pt black catalysts (in parenthesis, planes corresponding to characteristic diffraction signals of FCC Pt).

corresponding to the fcc crystal structure of Pt. Ru appears to be incorporated into the fcc structure of Pt because the diffraction peaks in PtRu are slightly shifted to higher 2θ values with respect to the same peaks in Pt. The diffraction peaks corresponding to (100), (101), (110), (103), and (201) planes of the Ru hexagonal close-packed crystal structure are not observed, thus indicating that if there is some Ru segregation from the PtRu nanocrystals, it is only present as amorphous material or it is in a very limited amount. The lattice parameters were calculated from the XRD patterns in Fig. 1, considering the diffraction peak positions of the Pt signals. The value for the PtRu black catalyst (3.877 Å) is lower than that of Pt black (3.918 Å), which indicates a contraction of the lattice due to the PtRu alloying to some extent [45]. Mean crystallite sizes, calculated from Scherrer's equation, were 2.3 ± 0.3 and 6.1 ± 0.7 nm for PtRu and Pt blacks, respectively. Then, the maximum theoretical metal surface areas were calculated assuming that such nanoparticles had a spherical shape, using the following equation:

$$SA = 6x10^3/\rho d \quad (1)$$

where SA is the surface area of the metallic nanoparticles ($m^2\,g^{-1}$); d is the mean crystallite size (nm), and ρ ($g\,cm^{-3}$) is the density of Pt or PtRu alloy ($\rho = \rho_{Pt} X_{Pt} + \rho_{Ru} X_{Ru}$, where $\rho_{Pt} = 21.45\,g\,cm^{-3}$, $\rho_{Ru} = 12.45\,g\,cm^{-3}$, and $X_{Pt(Ru)}$ are the weight percent of Pt and Ru in the catalyst) [46]. According to Eq. (1), the SA (Pt) is $45.8\,m^2\,g^{-1}$, which is in good agreement with the value reported by the manufacturer ($45-52\,m^2\,g^{-1}$). From EDX measurements, the Pt and Ru contents in PtRu black were 67.2 and 32.8 wt. %, respectively. Then, the maximum SA (PtRu) is $141\,m^2\,g^{-1}$, which is also in agreement with the value calculated from the analysis provided by the manufacturer ($129\,m^2\,g^{-1}$).

3.2. Influence of catalyst ink composition on the properties of anode catalyst layers

To assess the influence of catalyst ink composition, specifically the organic solvents used in its formulation, on the morphology and textural properties of catalyst layers, first of all inks were characterized by light scattering experiments. Fig. 2 shows the size distribution of agglomerates in the PtRu catalyst inks containing NBA or IPA as organic solvents (see Table 1). Two main peaks centred at around 1 μm and 10 μm were observed in both inks. Lim et al. [2] reported a similar result suggesting that peaks in the region below 1 μm were due to distributed sizes of Nafion® ionomer agglomerates in the dispersion solvents. This was further confirmed by studies of Nafion® aggregation, which depends on the dielectric constant and the solubility of solvents in water [13]. The Nafion® ionomer has polar parts and tends to aggregation

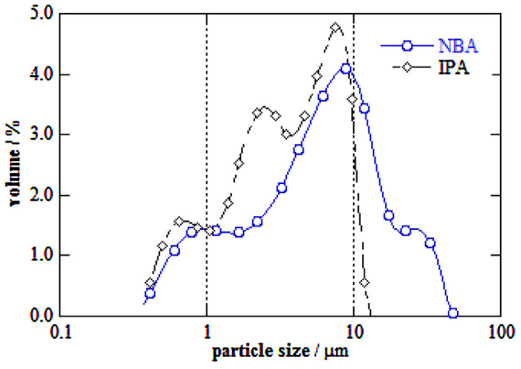

Fig. 2. Particle size distribution for the PtRu catalyst inks formulated with different organic solvents: (○) NBA and (◇) IPA.

when the polarity of the solvent decreases. This explains why the peak under 1 μm is centred at smaller size for IPA than for NBA, *i.e.* because the latter solvent has lower polarity than the former. On the other hand, peaks above 1 μm can be assigned to size distributions of agglomerates of the catalyst nanoparticles and Nafion®. It is clear from this figure that these agglomerates are larger when using NBA (note the peak centred at 26 μm). This can also be explained by the lower polarity of NBA, which favours larger-sized catalyst nanoparticles-Nafion® agglomerates.

It is expected that the size and compactness of the agglomerates will influence the morphology of the anode catalyst layer once the ink has been applied onto the substrate. Thus, the macroscopic changes in the morphology of the PtRu catalyst layers were examined by SEM. Fig. 3 shows the SEM images corresponding to the CLs prepared using NBA and IPA, respectively. It is shown in this figure that both CLs have granular-shape morphology, but it appears that the CL prepared using IPA is more compact and less porous than that prepared using NBA. Similar results were reported in the literature for catalyst layers made of supported catalysts [1,14]. In addition, a significant effect of the size of the catalyst agglomerates on the catalyst layer microstructure is expected. Consequently, to gain a better understanding on the microstructure of the anode catalyst layers in quantitative terms, pore size distributions were determined. Fig. 4 shows the pore size distributions corresponding to the PtRu catalyst layers prepared using NBA and IPA. Both curves show similar shape. However, in the region between 0.1–10 μm, the specific volume of the pores was higher for NBA than for IPA. It has been previously reported in the literature [1,5,6] that this region corresponds to the secondary pores, that is, the space existing between the agglomerates formed by the catalyst nanoparticles and Nafion®. Therefore, the secondary pore volume is larger by about 12% when NBA is used as organic solvent, in agreement with the morphology of the catalyst layers observed in Fig. 3.

3.3. Methanol oxidation on PtRu catalysed porous diffusion anodes

The activity of PtRu porous diffusion electrodes towards methanol oxidation was studied in three-electrode cell filled with $0.5\,mol\,dm^{-3}\,H_2SO_4 + 2.0\,mol\,dm^{-3}\,CH_3OH$ aqueous electrolyte. Fig. 5 shows the linear sweep voltammograms corresponding to methanol oxidation on catalyst layers in contact with the liquid electrolyte, by sweeping the potential from 0.075 to 0.750 V. The oxidation current given by the CL formulated with NBA as solvent was larger than that corresponding to the CL formulated with IPA. At low current densities, where no significant effect of mass transport and ohmic drop is expected, this can be at least partially explained by the different active surface areas of both catalyst layers. The ECSAs for CO stripping were determined to be 52.4 and $47.3\,m^2\,g^{-1}$ (using the conversion factor of $420\,\mu C\,cm^{-2}$ [43]), for the CLs made with NBA and IPA, respectively, *i.e.* by about 11% greater in the former. Note, however, that the current densities for NBA are much higher than this percentage when compared to IPA in the high current density part. This difference and the deviation from the exponential form in the potential range 0.55–0.70 V strongly suggest that there are transport limitation effects. This transport limitation is more apparent for IPA and could be explained considering the size and porosity of the agglomerates formed by the ionomer and the catalyst nanoparticles in both solvents, which are smaller in IPA (Fig. 2). The smaller porosity can limit the mass transport through the catalyst layer and therefore, the rate of the diffusion of the reactants to the catalyst sites and the rate of the removal of the reaction products from these points can be slowed down.

To obtain more insight into the properties of the catalyst layers, the PtRu catalysed surfaces were studied using the *eis* technique,

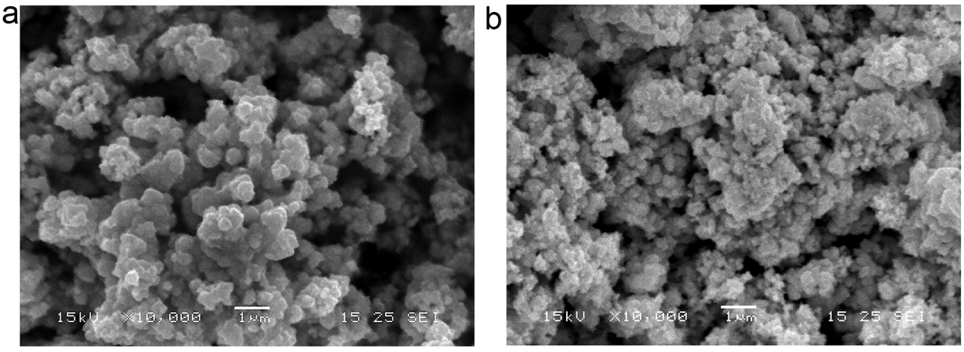

Fig. 3. SEM images of selected PtRu catalyst layers prepared using (a) NBA and (b) IPA as organic solvents.

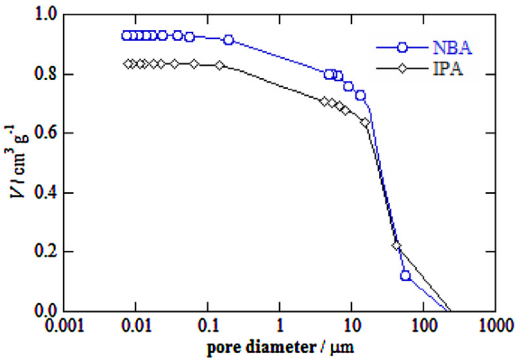

Fig. 4. Cumulative pore volume (*V*) *vs.* pore diameter curves for anode catalyst layers prepared from PtRu catalyst inks containing either (◯) NBA or (◇) IPA as organic solvent.

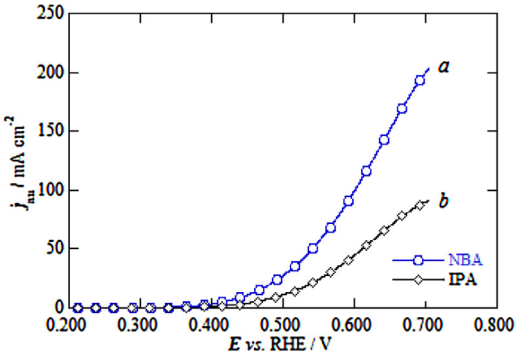

Fig. 5. *j-E* curves corresponding to the electrooxidation of methanol on PtRu black electrodes manufactured using (a) NBA and (b) IPA. 2.0 mol dm^{-3} CH_3OH + 0.5 mol dm^{-3} H_2SO_4. T = 20 °C. Sweep rate of 0.5 mV s^{-1}.

since the resistances associated with the methanol electrooxidation are included in impedance data and could be separated with the help of an appropriate equivalent circuit. Fig. 6 depicts the Nyquist plots corresponding to the PtRu catalysed anodes prepared using NBA and IPA. The impedance diagrams obtained at constant potential of 0.500 V showed similar features in both cases. They have the form of slightly depressed semicircles in the region of high and intermediate frequencies (1000-0.07 Hz), ending with an inductive loop at low frequencies. As shown in Fig. 6, the impedance values of the Nyquist plots corresponding to the CL formulated with NBA are smaller than those of the CL formulated with IPA. To gain more insight about this behaviour and its influence on the charge transfer of the methanol electrooxidation reaction, the impedance data have been interpreted by means of an equivalent circuit, assuming that this reaction proceeds via a two-step bifunctional mechanism [47]:

$$CH_3OH \rightarrow CO_{ads} + 4\,H^+ + 4\,e^- \quad (2)$$

$$CO_{ads} + H_2O \rightarrow CO_2 + 4\,H^+ + 4\,e^- \quad (3)$$

at which methanol is adsorbed mainly on Pt sites, while OH comes from the water dissociation on Ru sites, and CO being the main kinetically significant adsorbed intermediate on the catalyst. According to the kinetic theory derived by Armstrong and Henderson [48] and extended by Harrington, Conway [49] and Cao [50], for reactions involving one adsorbed intermediate, in which diffusion of participating species is not rate-limiting, different equivalent circuits can be used to interpret impedance data depending on the potential regions [51,52]. In the present context, considering that the mass transport effects are not relatively significant at 0.5 V, the most suitable equivalent circuit to interpret our *eis* results is depicted in Fig. 7, where R_Ω is the external ohmic resistance, which includes the uncompensated electrolyte resistance between the working and reference electrodes, the electronic resistance of the lead, and any contact resistance that may exist between the external surface of the electrode and the electrolyte; *CPE* is a constant phase element defined as [53]:

$$Z_{CPE} = 1/Y_0(i\omega)^m \quad (4)$$

where Y_0 is the admittance and m is the CPE exponent, represents the double layer capacitance, although porous surfaces can suffer a deviation from the ideal capacitive behaviour, indicated by the value of the frequency power; R_{ct} is the charge transfer of the electrode reaction, that is, how fast the rate of charge transfer changes with the change of the electrode potential which occurs without change in coverage; R_0 serves to modify the phase-delay according to reactions 2 and 3, and the inductance L means that the current signal follows a voltage perturbation with a phase delay, due to the slowness of CO_{ads} coverage relaxation [54]. The impedance diagrams can be fitted to the equivalent circuit shown in Fig. 7. The corresponding results are summarized in Table 2 and plotted together with the experimental data as solid lines in Fig. 6.

A comparison between the fitting data of Table 2 for both solvents points out to the physicochemical properties of the interphase related with the R_{ct}, R_0 and L elements as the main cause of the respective catalyst layer performances. The R_{ct} for methanol electrooxidation taking place at the catalyst-ionomer interface is smaller for the CL formulated with NBA than that formulated with IPA. This could be related to a higher electroactive surface area of the former. The relative active areas on both CLs can be estimated from impedance measurements through the determination of the double layer capacitance (C_{dl}), because the capacitance values are

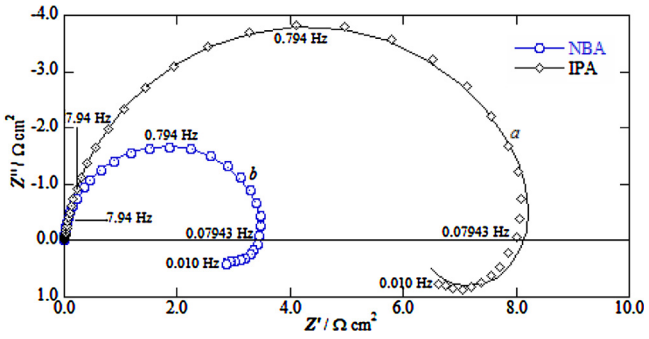

Fig. 6. Nyquist diagrams corresponding to methanol electrooxidation at 0.500 V on PtRu black electrodes manufactured using (◯) NBA and (◇) IPA. 2.0 mol dm^{-3} CH_3OH + 0.5 mol dm^{-3} H_2SO_4. T = 20 °C. The uncompensated resistance has been removed from the Nyquist diagrams. Solid lines correspond to fitting using the equivalent circuit shown in Fig. 7.

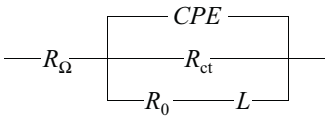

Fig. 7. Equivalent circuit used to interpret the impedance diagrams for the methanol electrooxidation on PtRu black catalysed diffusion anodes.

proportional to such active areas [55]. The values of C_{dl} estimated by Eq. (5) [56] are also shown in Table 1.

$$C_{dl} = Y_0(Y_0R_{ct})^{(1-n)/n} \quad (5)$$

The C_{dl} results indicate that the ECSA of the CL formulated with NBA is higher than that formulated with IPA, in good agreement with the results obtained from the CO stripping measurements. This clearly indicates that the secondary pores in the catalyst formulated with NBA make accessible a greater surface area of the catalyst. Furthermore, the anode reaction resistance ARR, which can be calculated from the expression [14]:

$$ARR = R_{ct} \times R_0/(R_{ct} + R_0) \quad (6)$$

is 2.64 Ω cm^2 for the CL formulated with NBA, but 6.33 Ω cm^2 for CL formulated with IPA, showing that methanol electrooxidation is enhanced in the former. On the other hand, R_0 and L are attributed to the adsorbed intermediates. The lower values corresponding to the CL formulated with NBA can be explained either by its higher number of reaction sites with respect to the CL formulated with IPA and/or by a faster oxidation rate of the intermediates in the former. To test the latter possibility, it is useful to determine the parameter τ^{-1}, the inverse of the coverage relaxation time, which is equivalent to the first order rate constant for the oxidative desorption of the intermediates [57]:

$$\tau^{-1} = R_0/L \quad (7)$$

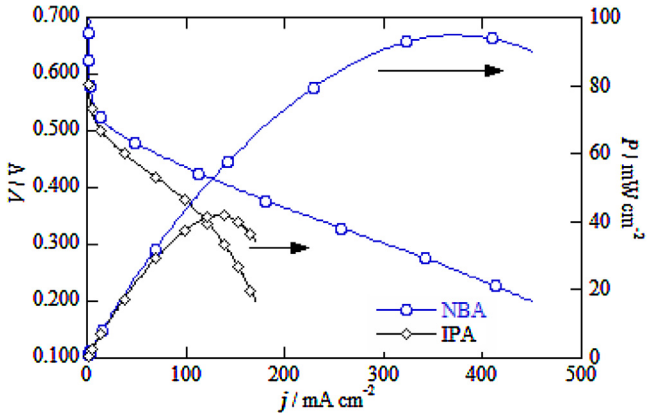

Fig. 8. *V-j* polarization and *P-j* curves for DMFCs with PtRu black catalysed anodes formulated with different inks containing: (◯) NBA and (◇) IPA. Cathodes catalysed with Pt black. T = 60 °C. [CH_3OH] = 2.0 mol dm^{-3}, fuel flow rate = 2 mL min^{-1}. Air flow rate = 100 mL min^{-1}.

This calculation gives τ^{-1} values of 0.158 and 0.162 s^{-1} for CLs formulated with NBA and IPA, respectively. This result suggests that the oxidation rate of the intermediates is similar in both CLs. Therefore, the different performance of the CLs prepared using NBA and IPA is due to the greater availability of the reaction sites in the former.

3.4. Single direct methanol fuel cell testing

Fig. 8 shows the polarization curves of MEAs in which the anode catalyst layers were formulated with NBA and IPA, denoted as MEA_{NBA} and MEA_{IPA}, respectively, the single DMFCs operating with 2 mol dm^{-3} CH_3OH aqueous solutions at 60 °C. The cathode feed was dry synthetic air at atmospheric pressure. It can be observed that the differences between current densities delivered by MEAs increase as the cell voltage decreases (thus delivering more current). The curvature tending to a limiting current density for the MEA_{IPA} shows mass transport limitation for currents much smaller than those obtained for MEA_{NBA}.

The current densities delivered by the MEAs prepared with NBA and IPA at the technically interesting voltage of 0.400 V were 148 and 85 mA cm^{-2}, equivalent to a power density of 59 and 34 mW cm^{-2}, respectively. The power density given by MEA prepared with NBA corresponds to an enhancement of approximately 74% compared with the MEA prepared with IPA. This suggests that the difference in DMFC performance is due solely to the anode catalyst layer in MEAs, because the compositions of the anode GDL, the membrane and the cathode were the same in both types of MEAs. A comparison between the MEA performances obtained in single DMFC (see Fig. 8) and previous results in the literature for active DMFCs [58–61] revealed that, in spite of the difference in the operating conditions and the MEA composition, the results presented in Table 3 are indicative of the good

Table 2
Fitting parameters obtained using the equivalent circuit of Fig. 7 for the methanol oxidation on the PtRu catalyst in the three-electrode cell.

solvent	R_Ω /Ω cm^2	Y_0 /Ω^{-1} s^n cm^{-2}	n	R_{ct}/Ω cm^2	R_0/Ω cm^2	L/H cm^2	C_{dl} /F cm^{-2}
NBA	0.251	0.05677	0.956	3.600	9.892	62.64	0.05277
IPA	0.378	0.02802	0.922	8.589	24.06	148.4	0.02484

Table 3
–Performances of single DMFCs using PtRu anode and Pt cathode unsupported catalysts at 0.400 V.

Methanol conc. /mol dm^{-3}	Oxidant (P /atm)	T_{cell} /°C	Anode loading /mg$_{PtRu}$ cm^{-2}	Cathode loading /mg$_{Pt}$ cm^{-2}	j /mA cm^{-2}	P /mW cm^{-2}	P_m /mW mg$_{(PtRu+Pt)}^{-1}$	Reference
0.5	Air (1.76)	60	8	6	155	62.0	4.40	[29]
1	Air (1)	64	3.9	2.3	76	30.4	4.90	[58]
1	Air (1.05)	55	10	8	141	56.5	3.11	[59]
1	Air (1)	80	3	2	200	80.0	16.0	[60]
2	Air (1)	60	4	4	148	59.0	7.40	This work

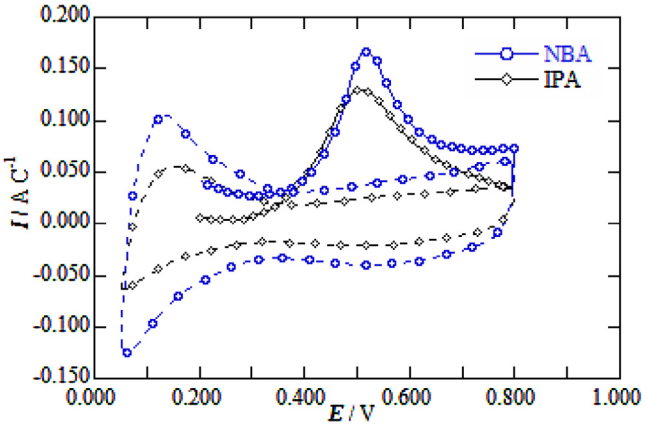

Fig. 9. CO stripping voltammograms for PtRu black catalysed anodes formulated with different inks containing: (◯) NBA and (◇) IPA after adsorption at 0.100 V vs. DHE. T = 25 °C. Anode fed with N_2; cathode with H_2. Both gases humidified with water at T_{cell}. Dashed lines are second scans (currents normalized by the CO_{ads} charge for better comparison).

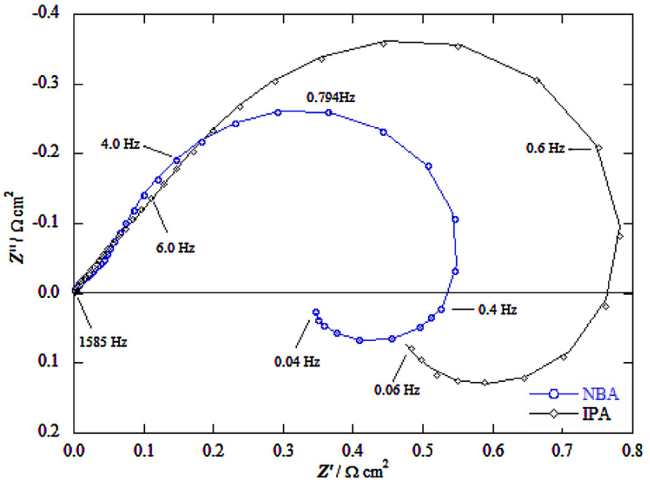

Fig. 11. Nyquist diagrams corresponding to the methanol electrooxidation in the anode of the DMFC. The PtRu anodes, fed with 2.0 mol dm^{-3} CH_3OH at 1.5 mL min^{-1}, were manufactured using (◯) NBA and (◇) IPA solvents at 60 °C. The Pt cathode, fed with H_2, served as the counter and the reference electrode. E = 0.400 V vs. DHE. The uncompensated resistance has been removed from the Nyquist diagrams.

performance delivered by the MEA made of the anode prepared using NBA.

The corresponding CO electrooxidation curves for the PtRu black catalysed anodes prepared using NBA and IPA are depicted in Fig. 9. It can be seen that both curves show the same profile; the CO oxidation peak potentials appeared at 0.510 and 0.517 V, for PtRu-IPA and PtRu-NBA, respectively, and the onset potentials for CO oxidation showed a little difference of 0.059 V, which are values comparable to those previously reported in the literature [62].

In order to see whether the catalyst crystallite size could contribute to the dramatic difference observed in the fuel cell performance, XRD spectra of PtRu catalysed anodes using NBA or IPA to prepare their catalyst layers, called PtRu-NBA and PtRu-IPA, respectively, were registered. Both diffractograms are shown in Fig. 10, together with that corresponding to PtRu black catalyst. The calculated mean crystallite sizes were 2.6 ± 0.7, 2.7 ± 0.6 and 2.3 ± 0.3 nm, for PtRu-NBA, PtRu-IPA and PtRu black catalyst, respectively. Therefore, there is no significant difference between crystallite sizes in the three specimens, thus indicating that sintering during catalyst ink after formation or MEA preparation can be excluded.

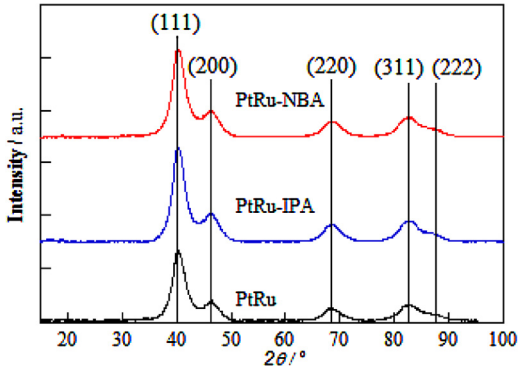

Fig. 10. X-ray diffraction patterns of PtRu black catalyst (in black), anode prepared with PtRu and IPA (in blue), and anode prepared with PtRu and NBA (in red) (in parenthesis, planes corresponding to characteristic diffraction signals of FCC Pt).

Furthermore, to get more insight about the influence of the anode catalyst layer on the MEA performance, we carried out an in situ *eis* analysis. Fig. 11 depicts the Nyquist plots corresponding to the PtRu black catalysed anodes, formulated using NBA and IPA, corresponding to MEAs in Fig. 8 at the technically interesting potential of 0.400 V *vs.* DHE. Both diagrams essentially show a kinetic control, being the methanol electrooxidation more favoured on the anode prepared using NBA. In addition, no mass-transport limitations due to methanol inlet feed are identified and the loops reflecting the inductive behaviour appear at the low frequency end of the impedance plots. The uncompensated resistances, R_Ω, are 0.200 and 0.212 Ω cm^2, respectively. Furthermore, the anodes used in DMFC usually have a high PtRu content. Consequently, the electrodes are thick and proton conductivity limitations in the catalyst layer could affect the MEA performance. Then, we estimated the proton resistance, R_p, from *eis* measurements in the anode catalyst layers in presence of methanol, to reflect the value close to the real operating conditions of the DMFC. To do this, we used the procedure described by Havránek and Wipperman [63], who adapted the transmission line equivalent circuit of a PEMFC cathode catalyst layer, for a DMFC anode catalyst layer. Briefly, Nyquist diagrams corresponding to

methanol oxidation should feature a linear slope at frequencies, ω, much higher than a "characteristic frequency", ω_c, defined as:

$$\omega_c = 1/(R_{MeOH}C_{pdl}) \quad (8)$$

where R_{MeOH} is the resistance of methanol oxidation, which considers the rate determining steps of methanol electrooxidation (the adsorption/dissociation of CH_3OH and the oxidation of adsorbed intermediates, like CO and COH), and C_{pdl} is a pseudo-double layer capacitance, which takes into account the importance of adsorbed intermediates (CH_3OH_{ad}, CO_{ad}, COH_{ad}, OH_{ad}, etc.) for the kinetics of methanol electrooxidation with a catalyst surface highly covered by adsorbed intermediates. The pseudo-layer capacitance can be obtained from the capacitive charging current of cyclic voltammograms of the methanol electrooxidation, according to:

$$C_{pdl} = j_{pdl} \times \nu^{-1} \quad (9)$$

where j_{pdl} is the pseudo-capacitative charging current density and ν is the scan rate. The linear slope, K, can be determined according to:

$$|Z| = K\omega^{-1/2} = \left(\sqrt{(R_p/C_{pdl})}\right)\omega^{-1/2} \quad (10)$$

where $|Z|$ is the impedance modulus and ω is the frequency of the harmonic signal. From the linear slope, the proton resistance of the catalyst, R_p, can be determined using the pseudo-double layer capacitance:

$$R_p = K^2 \times C_{pdl} \quad (11)$$

The specific proton conductivity of the catalyst layer is calculated from:

$$\sigma_p = d/AR_p \quad (12)$$

where d is the average thickness of the catalyst layer and A is the geometric area of the catalyst layer.

To determine the pseudo-double layer capacitances, C_{pdl}, cyclic voltammograms corresponding to the methanol electrooxidation on anodes prepared with different organic solvents, were registered in MEA environment at 0.002, 0.005, 0.010, and 0.020 V s^{-1}. The charging current density, j_{pdl}, was taken at an electrode potential of 0.200 V, at which the current density increased linearly with the scan rate. Values of C_{pdl} were calculated according to Eq. (9) and summarized in Table 4. Fig. 12 shows the modulus of the impedance, $|Z|$, *vs.* $\omega^{-1/2}$ of Nyquist diagrams in Fig. 11. Good straight lines with linear regression coefficient $r \geq 0.999$ were always found in the region of frequencies from 1258.92 to 7.94 Hz. This frequency range was chosen to minimize the influence of the faradaic process on $|Z|$. From these linear plots K and R_p values have been determined from Eqs. (10) and (11), respectively, and are also shown in Table 3. According to these results, the proton resistance in the anode catalyst layer formulated with NBA is about 43.4% lower than that in the anode catalyst layer formulated with IPA. This indicates that the accessible active sites, in a greater amount for NBA than for IPA, are well connected with the ionomers, so that the protons

Table 4
Fitting parameters obtained from the transmission line equivalent circuit for the methanol oxidation on a DMFC anode catalyst layer in the fuel cell [43].

solvent	C_{pdl} /F cm^{-2}	K /cm^2 $F^{-1/2}$	R_p /Ω cm^2
NBA	0.388	0.680	0.179
IPA	0.423	0.864	0.316

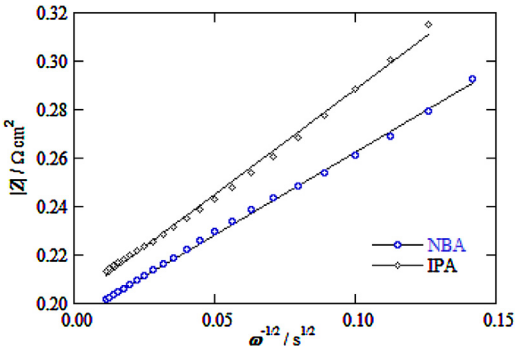

Fig. 12. $|Z|$ *vs.* $\omega^{-1/2}$ plots from impedance data taken from Fig. 9, corresponding to the PtRu black anodes manufactured using (◯) NBA and (◇) IPA solvents.

produced during the methanol oxidation with NBA can be easier transported from the active sites to the membrane.

4. Conclusion

The effect of the solvent in the preparation of non-supported PtRu catalyst inks with Nafion® and on the performance of the catalyst layers prepared with them for the methanol electrooxidation has been studied. Two solvents of different polarity, NBA and IPA, were tested. It is shown by light scattering that the catalyst inks prepared with NBA, less polar than IPA, are composed of PtRu-Nafion® agglomerates, which are greater in size than in the latter.

The SEM images of the prepared catalyst layers show granular-shape morphology both, for NBA and IPA. However, the catalyst layer prepared with NBA has higher porosity than the latter, as can be confirmed by the porosimetry. The secondary pore volume, corresponding to the space existing between the catalyst- Nafion® agglomerates (pore diameter in the range 0.01–10 μm), is larger by about 12% for NBA than for IPA.

The current density of the linear sweep voltammograms performed in the three-electrode cell, are higher for NBA, thus indicating a better use of the catalyst in this case and also a more favoured mass transport of reactants and products through the catalyst layer when compared to IPA, also explained by the higher porosity of the former.

The impedance results of the PtRu catalyst layers obtained also in the three-electrode cell at the technically interesting potential, interpreted with the help of an equivalent circuit, show higher double layer capacitance for NBA, in agreement with its higher active surface area. The specific oxidation rates of the intermediates appear to be the same in NBA and IPA and, therefore, the lower impedances in NBA can be mainly assigned to the greater availability of its active sites when compared to IPA.

The steady-state *V-j* polarization curves in single DMFCs with MEAs with PtRu and Pt catalysts in the anode and in the cathode, respectively, were obtained. It is shown that when the PtRu and Pt catalysts were prepared with NBA, the current densities were about twice when compared to the same cell with the PtRu catalyst being prepared with IPA, the mass transport limitations being more apparent in this latter case. Peak power densities of 95 and 40 mW cm^{-2} were obtained at current densities of 370 and 150 mA cm^{-2} for NBA and IPA, respectively, showing the better use of the catalyst in the former due to its higher porosity, in agreement with the three-electrode experiments.

The impedance experiments in the single DMFC when the Pt-catalysed cathode was fed with H_2, interpreted using the adapted transmission line equivalent circuit, were also in agreement with the conclusions above. The proton resistance in the anode catalyst layer formulated with NBA was about 43% lower than that with IPA,

thus indicating that the accessible active sites, in a greater amount for NBA, are well connected to Nafion® and easier transported from the active sites to the membrane for NBA than for IPA.

Acknowledgments

The authors gratefully acknowledge financial support given by the Spanish MINECO under project MAT2008-06631-C03-03/MAT.

References

[1] S.-J. Shin, J.-K. Lee, H.-Y. Ha, S.-A. Hong, H.-S. Chun, I.-H. Oh, Effect of the catalytic ink preparation method on the performance of polymer electrolyte membrane fuel cells, J. Power Sources 106 (2002) 146.
[2] C. Lim, R.G. Allen, K. Scott, Effect of dispersion methods of an unsupported Pt-Ru black anode catalyst on the power performance of a direct methanol fuel cell, J. Power Sources 161 (2006) 11.
[3] M. Uchida, Y. Fukuoka, Y. Sugawara, H. Ohara, A. Ohta, Improved preparation process of very-low-platinum-loading electrodes for polymer electrolyte fuel cells, J. Electrochem. Soc. 145 (1998) 3708.
[4] M. Chisaka, H. Daiguji, Effect of glycerol on micro nano structures of catalyst layers in polymer electrolyte membrane fuel cells, Electrochim. Acta 51 (2006) 4828.
[5] M. Uchida, Y. Aoyama, N. Eda, A. Ohta, New preparation method for polymer-electrolyte fuel cells, J. Electrochem. Soc. 142 (1995) 463.
[6] J. Lobato, M.A. Rodrigo, J.J. Linares, K. Scott, Effect of the catalytic ink preparation method on the performance of high temperature polymer electrolyte membrane fuel cells, J. Power Sources 157 (2006) 284.
[7] R.N. Bonifácio, J.O.A. Paschoal, M. Linardi, R. Cuenca, Catalyst layer optimization by surface tension control during ink formulation of membrane electrode assemblies in proton exchange membrane fuel cell, J. Power Sources 196 (2011) 4680.
[8] M. Chisaka, H. Daiguji, Effect of organic solvents on catalyst layer structure in polymer electrolyte membrane fuel cells, J. Electrochem. Soc. 156 (2009) B22.
[9] M. Chisaka, E. Matsuoka, H. Daiguji, Effect of organic solvents on the pore structure of catalyst layers in polymer electrolyte membrane fuel cells, J. Electrochem. Soc. 157 (2010) B1218.
[10] T.-H. Yang, Y.-G. Yoon, G.-G. Park, W.-Y. Lee, C.-S. Kim, Fabrication of a thin catalyst layer using organic solvents, J. Power Sources 127 (2004) 230.
[11] T.T. Ngo, T.L. Yu, H.-L. Lin, Influence of the composition of isopropyl alcohol/water mixture solvents in catalyst ink solutions on proton exchange membrane fuel cell performance, J. Power Sources 225 (2013) 293.
[12] M. Uchida, Y. Aoyama, N. Eda, A. Ohta, Investigation on the microstructure in the catalyst layer and effects of both perfluorosulfonate ionomer and PTFE-loaded carbon on the catalyst layer of polymer electrolyte fuel cells, J. Electrochem. Soc. 142 (1995) 4143.
[13] S. Wang, G. Sun, Z. Wu, Q. Xin, Effect of Nafion® ionomer aggregation on the structure of the cathode catalyst layer of a DMFC, J. Power Sources 165 (2007) 128.
[14] J.-H. Kim, H.-Y. Ha, I.-H. Oh, S.-A. Hong, H.I. Lee, Influence of the solvent in anode catalyst ink on the performance of a direct methanol fuel cell, J. Power Sources 135 (2004) 29.
[15] S. Tominaka, N. Akiyama, T. Momma, T. Osaka, An impedance analysis on properties of DMFC catalyst layers based on primary and secondary pores, J. Electrochem. Soc. 154 (2007) B902.
[16] F.-C. Wu, C.-C. Wan, Y.-Y. Wang, L.-D. Tsai, K.-L. Hsueh, Improvement of Pt-catalyst dispersion and utilization for direct methanol fuel cells using silane coupling agent, J. Electrochem. Soc. 154 (2007) B528.
[17] K.A. Sung, H.-Y. Jung, W.-K. Kim, K.-Y. Cho, J.-K. Park, Influence of dispersion solvent for catalyst ink containing sulfonated poly(ether ether ketone) on cathode behaviour in a direct methanol fuel cell, J. Power Sources 169 (2007) 271.
[18] M. Schonert, K. Jakoby, C. Schlumbohm, A. Gülsen, J. Mergel, D. Stolten, Manufacture of robust catalyst layers for the DMFC, Fuel Cells 4 (2004) 175.
[19] T.T. Ngo, T.L. Yu, H.-L. Lin, Nafion-based membrane electrode assemblies prepared from catalyst inks containing alcohol-water solvent mixtures, J. Power Sources 238 (2013) 1.
[20] Y. Zhu, J. Liang, C. Liu, T. Ma, L. Wang, Development of a passive direct methanol fuel cell (DMFC) twin-stack for long-term operation, J. Power Sources 193 (2009) 649.
[21] V. Baglio, A. Stassi, E. Modica, V. Antonucci, A.S. Aricò, P. Caracino, O. Ballabio, M. Colombo, E. Kopnin, Performance comparison of portable direct methanol fuel cell mini-stacks based on low-cost fluorine-free polymer electrolyte and Nafion membrane, Electrochim. Acta 55 (2010) 6022.
[22] T. Tsujiguchi, M.A. Abdelkareem, T. Kudo, N. Nakagawa, T. Shimizu, M. Matsuda, Development of a passive direct methanol fuel cell stack for high methanol concentration, J. Power Sources 195 (2010) 5975.
[23] Y. Kim, D. Shin, J. Seo, N. chang, H. Cho, Y. Kim, S. Yon, System integration of a portable direct methanol fuel cell and a battery hybrid, Int. J. Hydrogen Energy 35 (2010) 5621.
[24] Y. Na, J. Suh, I. Song, K.-H. Choi, H. Choi, K.B. Kim, J.-Y. Park, Stable operation of air-blowing direct methanol fuel cell stacks through uniform oxidant supply by varying fluid flow fixtures and developing the flow sensor, Int. J. Hydrogen Energy 36 (2011) 9205.
[25] Z. Yuan, Y. Zhang, J. Leng, Y. Gao, X. Liu, Development of 4-cell air-breathing micro direct methanol fuel cell stack, J. Power Sources 202 (2012) 134.
[26] S. Tanaka, Fuel cells and their components based on microsystem technology, WIREs Energy Environ 2 (2013) 350.
[27] M.K. Rashed, M.A.M. Salleh, H.A. Abdulbari, M.H.S. Ismail, S. Izhar, The effects of electrode and catalyst selection on microfluidic fuel cell performance, ChemBioEng Rev. 2 (2015) 356.
[28] N.K. Shrivastav, S.B. Thombre, R.B. Chadge, Liquid feed passive direct methanol fuel cell: challenges and recent advances, Ionics 22 (2016) 1.
[29] X. Ren, Performance of direct methanol fuel cells for portable power applications, in: P. Barbaro, C. Bianchini (Eds.), Catalysis for sustainable energy production, Wiley-VCH Verlag GmbH & Co. KGaA, Weinheim (Germany), 2009, pp. 47–69 Ch. 2.
[30] A. Mehmood, M.A. Scibioh, J. Prabhuram, M.-G. An, H.Y. Ha, A review on durability issues and restoration techniques in long-term operations of direct methanol fuel cells, J. Power Sources 297 (2015) 224.
[31] E.S. de Castro, Facilitated direct liquid fuel cells with high temperature membrane electrode assemblies, 2015 U.S. Department of Energy Hydrogen and Fuel Cells Program and Vehicle Technologies Office Annual Merit Review and Peer Evaluation Meeting, Arlington, Virginia, 8–12 June, 2015.
[32] L. Zou, J. Guo, J. Liu, Z. Zou, D.L. Akins, H. Yang, Highly alloyed PtRu black electrocatalysts for methanol oxidation prepared using magnesia nanoparticles as sacrificial templates, J. Power Sources 248 (2014) 356–362.
[33] J. Wang, R.F. Savinell, Simulations studies on the fuel electrode of a methanol air polymer electrolyte fuel cell, in: S. Srinivasan, D.D. Macdonald, A.C. Khandkar (Eds.), Proceedings of the symposium on Electrode material for Energy Conversion and Storage PV 94-23, The Electrochemical Society Proceedings Series, Pennington, NJ, 1994, pp. 326.
[34] J. Guo, G. Sun, S. Sun, S. Yan, W. Yang, J. Qi, Y. Yan, Q. Xin, Polyol-synthesized PtRu/C and PtRu black for direct methanol fuel cells, J. Power Sources 168 (2007) 299.
[35] Y.-M. Tsou, L. Cao, M. Young, J. Morse, Approaches to improve durability & special applications of FC MEAs, ECS Trans 19 (2009) 47.
[36] F. Alcaide, G. Álvarez, P.L. Cabot, H.-J. Grande, O. Miguel, Effect of gas diffusion layer composition on the performance of direct methanol fuel cells, Electrochemical and Solid-State Letters 13 (2010) B73.
[37] S.C. Thomas, X. Ren, S. Gottesfeld, Influence of ionomer content in catalyst layers on direct methanol fuel cell performance, J. Electrochem. Soc. 146 (1999) 4354.
[38] P. Zelenay, X. Ren, S.C. Thomas, J. Davey, S. Gottesfeld, Catalysts inks and method of application for direct methanol fuel cells, W00245188, 2002.
[39] D. Chu, R. Jiang, Effect of operating conditions on energy efficiency for a small passive direct methanol fuel cell, Electrochim. Acta 51 (2006) 5829.
[40] V. Baglio, A. Stassi, F.V. Matera, V. Antonucci, A.S. Aricò, Investigation of passive DMFC mini-stacks at ambient temperature, Electrochim. Acta 54 (2009) 2004.
[41] F. Alcaide, G. Álvarez, O. Miguel, M.J. Lázaro, R. Moliner, A. López-Cudero, J. Solla-Gullón, E. Herrero, A. Aldaz, Pt supported on carbon nanofibers as electrocatalyst for low temperature polymer electrolyte membrane fuel cells, Electrochem. Comm. 11 (2009) 1081.
[42] A. Weibel, R. Bouchet, F. Boulc'h, P. Knauth, The big problem of small particles: a comparison of methods for determination of particle size in nanocrystalline anatase powders, Chem. Mater. 17 (2005) 2378.
[43] T. Vidaković, M. Christov, K. Sundmacher, The use of CO stripping for in situ fuel cell catalyst characterization, Electrochim. Acta 52 (2007) 5606.
[44] F. Alcaide, G. Álvarez, N. Tsiouvaras, M.A. Peña, J.L.G. Fierro, M.V. Martínez-Huerta, Electrooxidation of H_2/CO on carbon-supported PtRu-MoO_x nanoparticles for polymer electrolyte fuel cells, Int. J. Hydrogen Energy 36 (2011) 14590.
[45] D. Chu, S. Gilman, Methanol electro-oxidation on unsupported Pt-Ru alloys at different temperatures, J Electrochem Soc 143 (1996) 1685.
[46] A.S. Aricò, P.L. Antonucci, E. Modica, V. Baglio, H. Kim, V. Antonucci, Effect of Pt-Ru alloy composition on high-temperature methanol electro-oxidation, Electrochim. Acta 47 (2002) 3723.
[47] M. Watanabe, S. Motoo, Electrocatalysis by ad-atoms: Part II. Enhancement of the oxidation of methanol on platinum by ruthenium ad-atoms, J. Electroanal. Chem. 60 (1975) 267.
[48] R.D. Armstrong, M. Henderson, Impedance plane display of a reaction with an adsorbed intermediate, J. Electroanal. Chem. 39 (1972) 81.
[49] D.A. Harrington, B.E. Conway, ac Impedance of Faradaic reactions involving electrosorbed intermediates-I. Kinetic theory, Electrochim. Acta 32 (1987) 1703.
[50] C.-N. Cao, On the impedance plane displays for irreversible electrode reactions based on the stability conditions of the steady-state-I. One state variable besides electrode potential, Electrochim. Acta 35 (1990) 831.
[51] G. Wu, L. Li, B.-Q. Yu, Effect of electrochemical polarization of PtRu/C catalysts on methanol electrooxidation, Electrochim. Acta 50 (2004) 1.
[52] F. Seland, R. Tunold, D.A. Harrington, Impedance study of methanol oxidation on platinum electrodes, Electrochim. Acta 51 (2006) 3827.
[53] A. Lasia, Electrochemical impedance spectroscopy and its applications, in: B.E. Conway, R.E. White, J. O'M. Bockris (Eds.), Modern Aspects of Electrochemistry, Kluwer Academic/Plenum Publishers, New York, NY, 1999, pp. 143 no. 32.
[54] J.T. Müller, P.M. Urban, W.F. Hölderich, Impedance studies on direct methanol fuel cell anodes, J. Power Sources 84 (1999) 157.

[55] D. Chakraborty, I. Chorkendorff, T. Johannessen, Electrochemical impedance spectroscopy study of methanol oxidation on nanoparticulate PtRu direct methanol fuel cell anodes: Kinetics and performance evaluation, J. Power Sources 162 (2006) 1010.
[56] J. Brug, A.L.G. Van den Eeden, M. Sluyters-Rehbach, J.H. Sluyters, The analysis of electrode impedances complicated by the presence of constant phase element, J. Electroanal. Chem. Interfacial Electrochem 176 (1984) 275.
[57] R.E. Melnick, G.T.R. Palmore, Impedance spectroscopy of the electro-oxidation of methanol on polished polycrystalline platinum, J. Phys. Chem. B 105 (2001) 1012.
[58] H. Dohle, H. Schmitz, T. Bewer, J. Mergel, Development of a compact 500 W class direct methanol fuel cell stack, J. Power Sources 106 (2002) 313.
[59] C. Xie, J. Bostaph, J. Pavío, Development of a 2 W direct methanol fuel cell power source, J. Power Sources 136 (2004) 55.
[60] J. Prabhuram, N.N. Krishnan, B. Choi, T.-H. Lim, H.Y. Ha, S.-K. Kim, Long-term durability test for direct methanol fuel cell made of hydrocarbon membrane, Int. J. Hydrogen Energy 35 (2010) 6924.
[61] P. Joghee, J.N. Malik, S. Pylypenko, R. O'Hayre, A review on direct methanol fuel cells −In the perspective of energy and sustainability, MRS Energy & Sustainability 2 (2015) 1.
[62] H.N. Dinh, X. Ren, F.H. Garzon, P. Zelenay, S. Gottesfeld, Electrocatalysis in direct methanol fuel cells: in-situ probing of PtRu anode catalyst surfaces, J. Electroanal. Chem. 491 (2000) 222.
[63] A. Havránek, K. Wippermann, Determination of proton conductivity in anode catalyst layers of the direct methanol fuel cell (DMFC), J. Electroanal. Chem. 57 (2004) 305.